Progress In Electromagnetics Research M, Vol. 75, 167–178, 2018

An Advanced Electrical Properties Measurement Approach with a Designed Bi-Static Ultra-Wideband Impulse Radar Sensor

Younes Ahajjam[1, 2, *], Otman Aghzout[2, 3], Josè M. Catala-Civera[1], Felipe Peñaranda-Foix[1], and Abdellah Driouach[2]

Abstract—This paper reports on the development of a compact, low-cost, impulse bi-static UWB radar sensor for its use as non-destructive methods for electrical property measurement in industrial application. This UWB Radar sensor consists of an ultrashort-monocycle-pulse transmitter of 330 ps, an oscilloscope as a UWB sampling receiver with a high wide band of 6 GHz, and two UWB antennas ranging from 0.4 to 6 GHz. A new model of SRD has been introduced to decrease the rise time of the impulse. Performance of this UWB radar sensor was verified through two kinds of applications: range detection and electrical property measurements. All measurements have been carried out in an anechoic chamber with a distance variation between 80 and 300 cm. The full radar system provides good agreement between the experimental and theoretical results, which demonstrate its application in many fields, especially for electrical Property Measurements.

1. INTRODUCTION

Nowadays, an accurate measurement of the electrical properties of materials is very important. Because each material has a unique electrical characteristic, this electrical property establishes the material behaviour with the presence of EM fields. In addition, an accurate measurement of this property provides valuable information to incorporate this material in applications [1, 2], to be able to perform a specific design [3, 4] or to monitor some industrial processes [5, 6]. Moreover, the importance of these properties is due also to a direct correlation with other principal parameters, such as viscosity, curing degree, and the percentage of humidity. Actually, there are many methods in the characterization dielectric of materials. All these methods can be summarized into four principal groups: techniques based on concentrated circuits, techniques based on transmission lines, techniques based on resonant cavities, and techniques based on free space propagation. The techniques based on free space propagation consist normally in a designed Radar Sensor. A designed UWB Radar Sensor presents many advantages: it is a nondestructive and noninvasive method, able to penetrate materials without any alteration or contamination. This advantage makes them a very attractive solution for a measurement of the internal property in inhomogeneous or granular materials. In addition, the UWB radar sensor gives a lot of accuracy in measurements and has less dependency on the exterior conditions, like temperature or humidity. Recently, the interest in UWB radar sensors systems for non-destructive application has increased significantly [7–10]. Numerous systems work in the time domain and have an effective UWB frequency spectrum around 0.1 GHz to 10 GHz [10, 11]. The principal part of any UWB radar sensors is a UWB nanosecond pulse generator. The UWB radar sensors system described in this work is composed by a designed UWB impulse generators part, two UWB antennas, and an oscilloscope as a receiver.

Received 3 July 2018, Accepted 13 September 2018, Scheduled 12 November 2018

* Corresponding author: Younes Ahajjam (ahajjam.younes@gmail.com).

[1] Instituto ITACA, Universitat Politcnica de Valncia. Camino de Vera s/n, Valencia 46022, Espaa. [2] Department of Physics, Faculty of Science, UAE Abdelmalek Essaadi University, Tetouan, Morocco. [3] Department of Telecommunication, ENSA, UAE Abdelmalek Essaadi Univertisy, Tetouan, Morocco.

The UWB pulses were generated by an avalanche transistor and sharpened by a step recovery diode. Normally in the literature, there are many techniques focused on generating a nanosecond monocycle UWB pulses [12–17]. In most of these articles, the monocycle pulse amplitude is limited, presents a lot of ringing and does not satisfy the criteria of a good radar sensor, especially when the electrical property is at stake. Therefore, the output pulse of the radar system must be improved, e.g., has a great amplitude with little ringing, because an extra-level in ringing in the output waveform involves more distortion and presents more difficulties to extract information regarding the data processing. For this reason, a useful technique consists in modelling the SRD has been used, and the new model of SRD has been inserted in AWR Microwave office and Multisim. Then the simulation accuracy has been improved, and the rise time has been decreased from 530 ns to 330 ns. This technique leads also to decreasing the ringing in the output pulse. However, unlike the UWB Monocycle impulses generator described in some bibliographical results [17, 18], the generator depicted in this paper presents the advantage of producing monocycle pulses with a reasonably high output amplitude with low ringing levels. These two advantages will make the measurements in very accuracy state. In order to validate the performance of this system, two kinds of measurements have been presented. The first one consists of measuring the distance of the range target, while the second one consists of measuring the electrical property of materials. All measurement has been carried out in an anechoic chamber in which disturbance of parasitic signals is avoided, and the distance of target was varied from 80 to 300 cm. The pulse generator circuit is completely fabricated on the microstrip structure, which has the characteristic of compactness and small size. A good agreement between the measured and calculated results was achieved.

2. RADARS SYSTEM DESCRIPTION

Normally, there are two main configurations in the systems of radar, the bi-static and mono-static configurations [19]. Compared with the bi-static configuration, the mono-static one presents many disadvantages and needs more technical requirements for accuracy measurements. For this reason in this paper we have chosen the bi-static configuration to get accurate and efficient results. In Fig. 1, the whole system in bi-static configuration is presented. To avoid any perturbations and interferences during the measurements, the separating distance between the transmitting Tx and receiving antenna Rx is fixed at 25 cm. On the other hand, we consider that (0, 0) is the origin position located at half distance separating the antennas used in the experiments, while d is the distance from the origin position to the target.

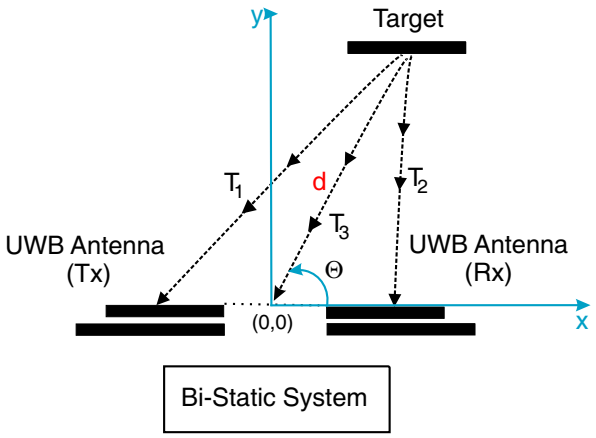

Figure 1. Bi-static system configuration and measurement setup.

The overall radar system consists of two antennas with a wide bandwidth, an oscilloscope as a receptor and the proposed, designed UWB monocycle impulse generator. A central challenge in the design of a UWB radar sensor system is the availability of a pulse source with high peak power and short rise-time, knowing that the characteristic of the UWB pulse generator establishes the entire

performance of the radar system. However, a monocycle pulse was selected over a Gaussian pulse because it has a narrow bandwidth, and does not contain the DC current, hence, provides little loss in the antennas, because of the UWB antennas used in these measurements ranging 0.4–6 GHz and 0.6–6 GHz, respectively. Therefore, the monocycle is very appropriate in our Radar sensor applications. The circuit schematic of the proposed impulse generator is shown in Fig. 2. It is constructed by three principal parts: avalanche transistor circuit, SRD pulse sharpener circuit, and monocycle forming network.

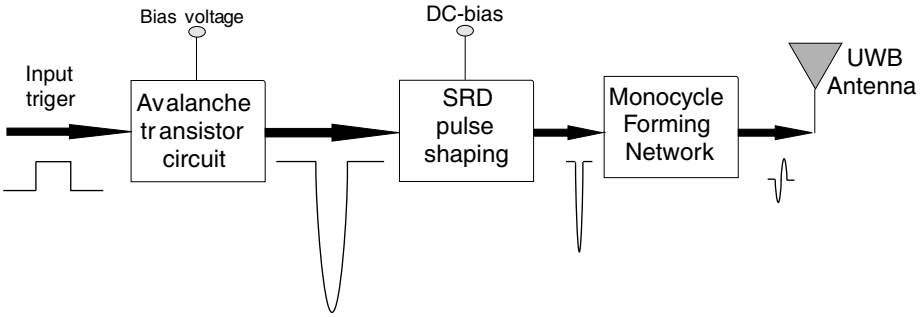

Figure 2. Circuit diagram of the proposed Gaussian pulse generator.

The first part of the generator consists of Q, $C1, R1, C2$, and $R2$ as shown in Fig. 3. The Q used in this work is an MMBT2222A, which is a bipolar (BJT) transistor with NPN junction, characterized by a maximum of Interruption voltage collector-emisor of 40 V, $Ic = 1$ A, a transition frequency of 300 MHz, and a maximal power of 350 mW with a surface Mount SOT-23-3. The correspondent capacitance and resistance components are as follows: $C1 = 1100$ pf, $C2 = 50$ pf, $R1 = 50\,\Omega$, $R2 = 50\,\Omega$, $R3 = 50\,\mathrm{K}\Omega$. The detailed description of the generator can be found in [20].

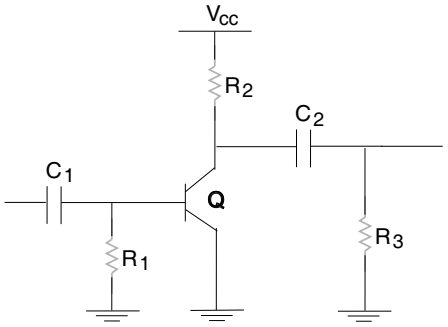

Figure 3. Circuit designed for the avalanche transistor circuit.

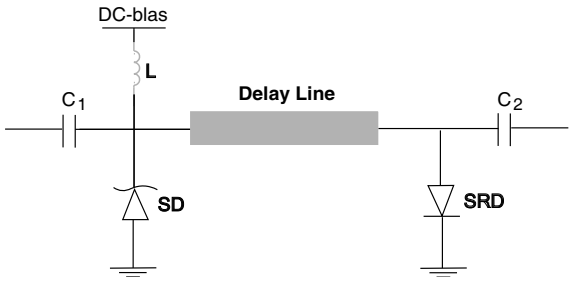

Figure 4. Circuit designed for the SRD pulse sharpening circuit.

The second part of the generator consists of an SRD pulse sharpening, the entire network as shown in Fig. 4.

First, the SD used is an SMD110PL-TP, which is a SOD-123FL with an operating temperature ranging from $-55°$C to $+125°$C, a storage temperature ranging from $-55°$C to $+150°$C, a maximum recurrent peak reverse voltage and maximum DC blocking voltage of 100 V, an average forward current of 1.0 A, and a maximum instantaneous forward voltage of 0.85 V. Secondly, the SRD is MA44769-287T. The elected SRD has a reverse capacitance of 1 pF, a minority-carrier lifetime of 10 ns, a minimum transition time of 150 ps, a reverse breakdown voltage of 30 V, a forward bias current of 50 mA and a SOD323 package. Finally, the corresponding values of the capacitances and inductance are: $C1 = 50$ pf, $C2 = 50$ pf and $L = 100$ uH. More detailed description can be encountered in work presented in [20]. On the other hand, there is a useful technique in design. This technique shorts the discharge path as short as possible; therefore, a minimum of the ringing is obtained in the output pulse, around 3.6% in

overshoot.

The SRD has a crucial role in our generator circuits, ever since the computer simulation of an SRD is a challenging question. This challenge consists in the great difference between the SRD and classical PN junction, since in the conventional time domain Simulator like AWR Microwave office and Multisim Simulators, advanced SRD models are not yet implemented. To face the challenge described above, a new model of SRD has been proposed. The choice of this model has been decided after studying many models existing in the literature. One of the advantages of this model is to increase the rise time. Fig. 5 shows the elected voltage-switch model of SRD and its corresponding equivalent circuit, where Rs is the nonlinear resistor and Cj the nonlinear capacitor, while Ls and Cp represent parasitic parameters of the SRD component.

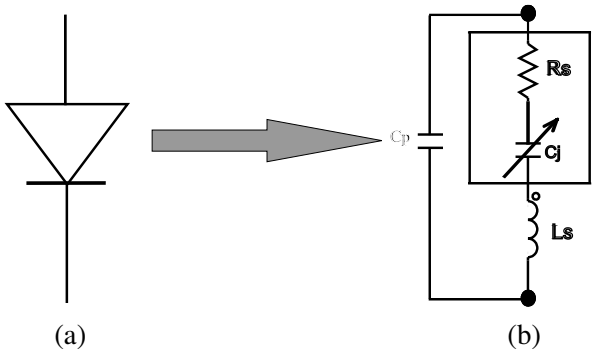

Figure 5. (a) SRD of AWR Microwave office. (b) A new model of step recovery diode (SRD).

The simulation results are shown in Fig. 6, where Fig. 6(a) is the output waveform using the usual SRD proposed by the AWR Microwave Office Design Suite, while the output waveform in Fig. 6(b) was generated when the SRD model described below was applied. The simulations were realized with the HSPICE transient simulator included in the AWR Microwave Office design suite. The SRD in both results was connected to the output of the microstrip with a 10 mm in the delay line and 90 Ω in characteristic impedance. The connection of the SRD at the length of the delay line was chosen with the aim to get the highest possible output amplitude. The generated Gaussian pulses are −6 V in amplitude and approximately 180 ps FWHM (Full-Width at Half Maximum) in width. Fig. 6 shows how the new model of SRD affects the behaviour of the output waveform of the circuit. The effect of this new model includes removing the most ringing occurring just after the descent of the pulse and leads us to more understanding of the significant role played by the SRD diode in the formation final of the Gaussian pulse. The generated Gaussian pulses have −6 V in amplitude with 3.6% in overshoot.

The SRD in both results was connected to the input of the microstrip with a 10 mm in the delay line and 90 Ω in characteristic impedance.

The choice of 90 Ω has been made because the upper value from 150 Ω gives a deformed output pulse, and the lower value than 50 Ω decreases the amplitude of the output waveform pulse. In this work, many simulations and measurements have been done with different values ranging from 50 to 150 Ω to lead to the optimal impedance providing optimal responses. Therefore, a 90 Ω delay line has been chosen as an alternative to this paradox. Physically, the impact of variation impedance value on the behaviour of the pulse can be explained by two cases.

In the first case, the lower impedances force the pulse to circulate quickly, which causes pulse accumulations of the going and returning pulses. Obviously, the given output waveform decreases. In the second case, higher impedances force the pulse to circulate slowly, which causes an accumulated pulses with a phase shift of time, producing a deformed output waveform.

The connection of the SRD at the length of the delay line was chosen with the aim to get the highest possible output amplitude. The generated Gaussian pulses are −6 V in amplitude and approximately 180 ps FWHM (Full-Width at Half Maximum) in width. A significant difference between the output waveforms of the circuit before and after inserting the new model of SRD can be clearly seen in Fig. 6. This difference consisting in removing the most ringing happenning just after the descent of the pulse,

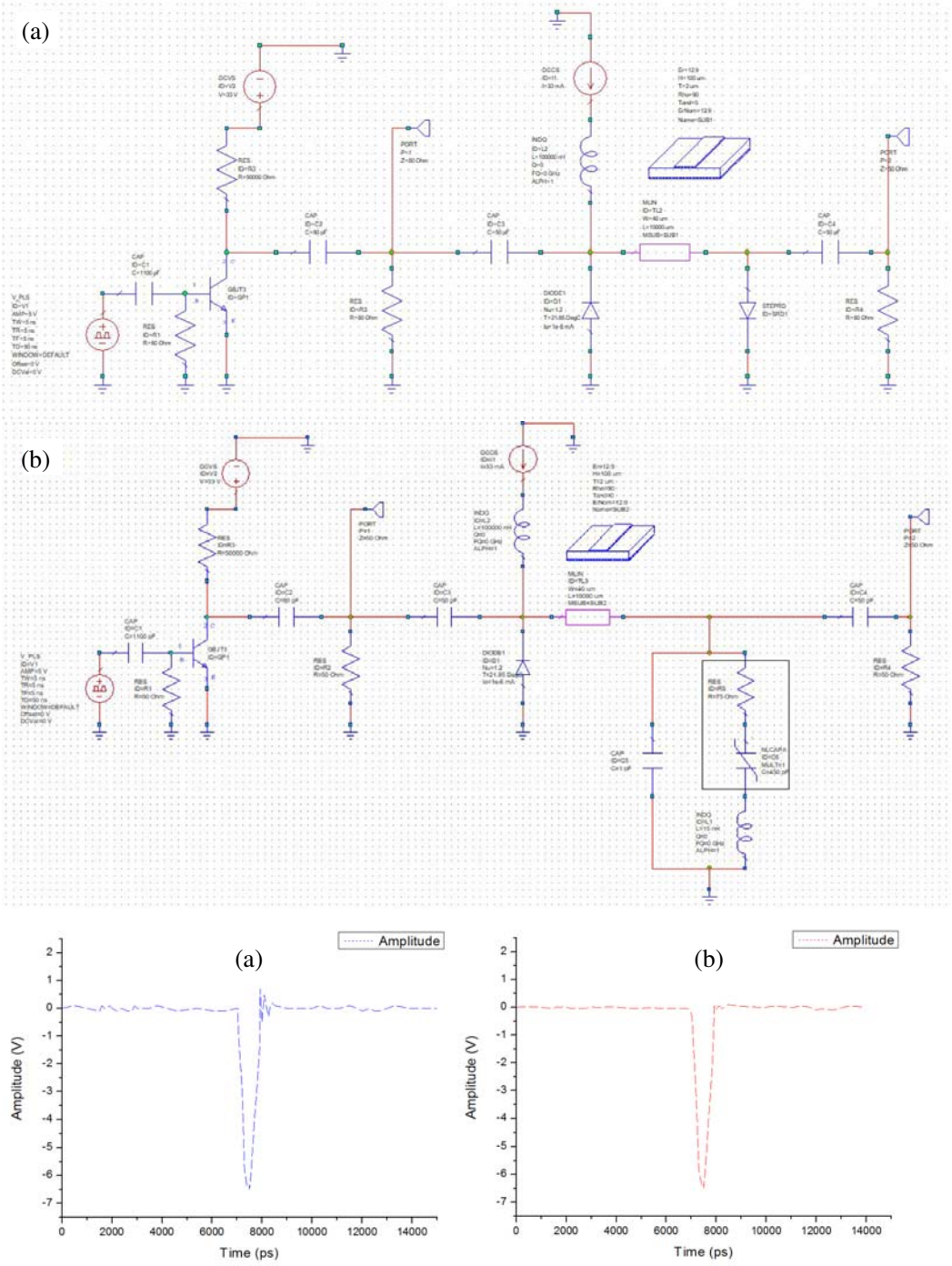

Figure 6. Simulation model with AWR of the output waveform with (a) and without (b) the application of the new model of SRD respectively.

which leads us to more understanding of the enormous roles played by the SRD diode in the formation final of the Gaussian pulse. The generated Gaussian pulses have −6 V in amplitude with 3.6% in overshoot.

In order to find a commercial step recovery diode that acts similarly to our proposed model described above, many experiments have been done with different SRDs. Finally, the diode MA44769-287T has been elected and implemented in the final design of the impulse generator. Fig. 7 shows the output result

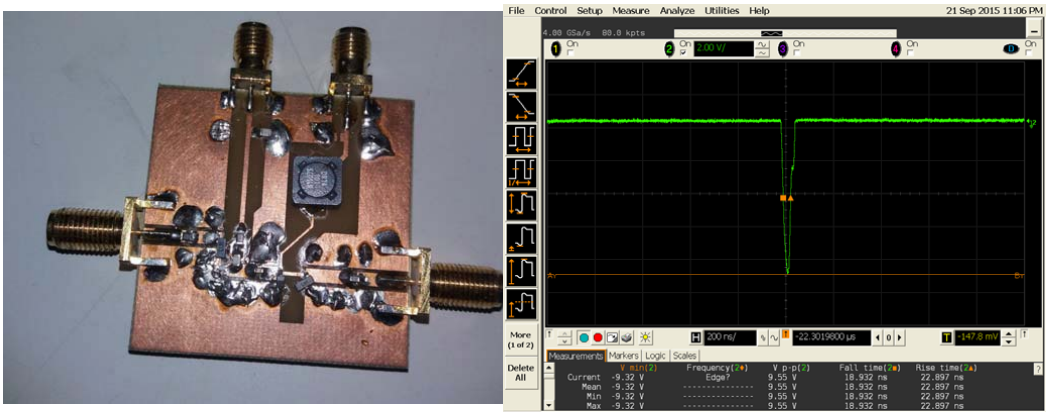

Figure 7. Fabricated circuit using the diode MA44769-287T and the measured output waveform results.

of the diode MA44769-287T. The MA44769-287T has a reverse capacitance of 1 pF, a minority-carrier lifetime of 10 ns, a minimum transition time of 150 ps, a reverse breakdown voltage of 30 V, forward bias current 50 mA and a SOD323 package.

3. MEASUREMENTS

For the purpose to validate the performance of the designed monocycle pulse described above, some measurements have been made. In all experiments, the designed monocycle pulse was triggered by a quadratic pulse generator, and this trigger pulse has 5 V in amplitude and rise time of 5 ns. After that, the monocycle generated has been transmitted by a UWB TX antenna directly toward a target, and the reflected pulse was received by a UWB RX antenna. The result in the time domain has been shown on the screen of the oscilloscope. Finally, the control in real time of the whole experiment has been made with a developed program in LabVIEW. The quadratic pulse generator used in this experiement is the 8112A 50 MHz Programmable Pulse Generator, while the oscilloscope is Agilent Infiniium 8000 Series. The developed radar sensor was constructed in bi-static configuration. The measurement setup of the sensor is shown in Fig. 8. To respect the principles of electromagnetic compatibility and to avoid any parasitic signal between the transmitter (Tx) and receiver (Rx), the separation distance between them has been chosen at 25 cm for all measurements.

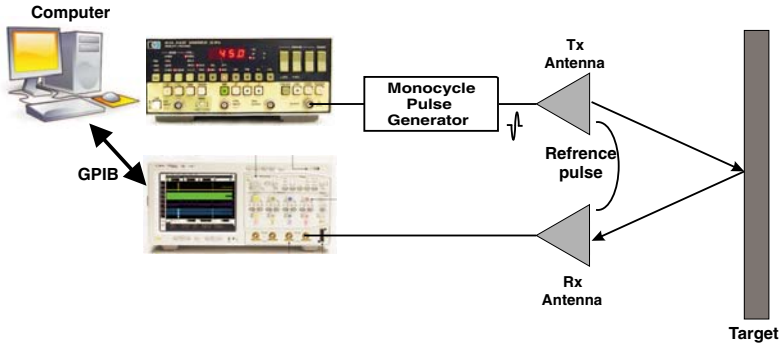

Figure 8. Diagram and setup of the whole system measurement.

3.1. Measurements Range Distance

The designed system has been tested firstly for a distance measurement towards a horizontal perfect electric conductor; the choice of metal as a target has been used to get the maximum EM energy in

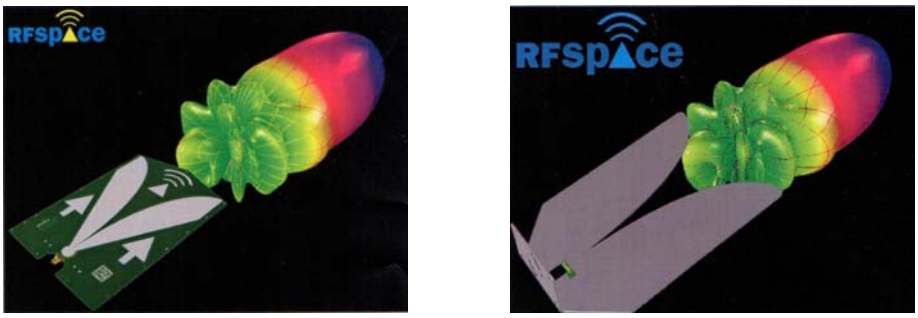

Figure 9. Photograph of the UWB antennas with the radiation pattern.

Figure 10. Photograph of measurement setup and a photograph of UWB impulse generator.

the reception. The metal plate used in this experiment has a width with a size of 30 cm × 70 cm × 3 mm. The distances separating the target metal plate and the antennas ranged from 80 cm to 300 cm. The measurements of the distance range have been made using the Time-of-Flight principle (ToF), and a high voltage pulses with an amplitude of 6.4 V at 50 Ω. Fig. 9 shows the antennas used in this measurements; they are two UWB commercial antennas from RFSPACE Inc. The first one, TSA600-6000, is a PCB with a wide band from 0.6 GHz to 6 GHz, while the second one, Tapered Slot Antenna, is aluminum with a wide band from 0.43 GHz to 6 GHz. The two antennas have a linear polarisation with excellent gain over the entire range, low VSWR over full range with no resonances, a clean impulse response, which make them very appropriate for our radar sensor applications.

The distance of the target at 80, 180 and 300 cm has been fixed to compare the responses of these two antennas used in the experment and to confirm the performances operability of the designed system prototype. The measurements setup of the pulse radar sensor for the selected target distance is shown in Fig. 10, while the time-domain response of the radar sensor measurement towards the metal plate is shown in Fig. 11.

We observe, clearly from the behaviour of the curve, the presence of the reference pulse and the reflected pulse from the object. The reflected pulse was accompanied with some unwanted peaks and some ringing, and this unwanted ringing occurred after the target return was received. The first pulse is due to coupling antennas transmission, while the second one is the reflected pulse from the material of the target. This reflected pulse approaches or moves away from the main pulse proportionally with the movement of the targets. From the results obtained above, it seems that the first antenna Tapered Slot Antenna gets a great result regarding transmission and gives pulses with a minimum of ringing. Generally, in time-domain measurement, a UWB antenna that begins from lower frequencies gives more accuracy than that begins from high frequencies. Therefore, designing a UWB antenna ranging from

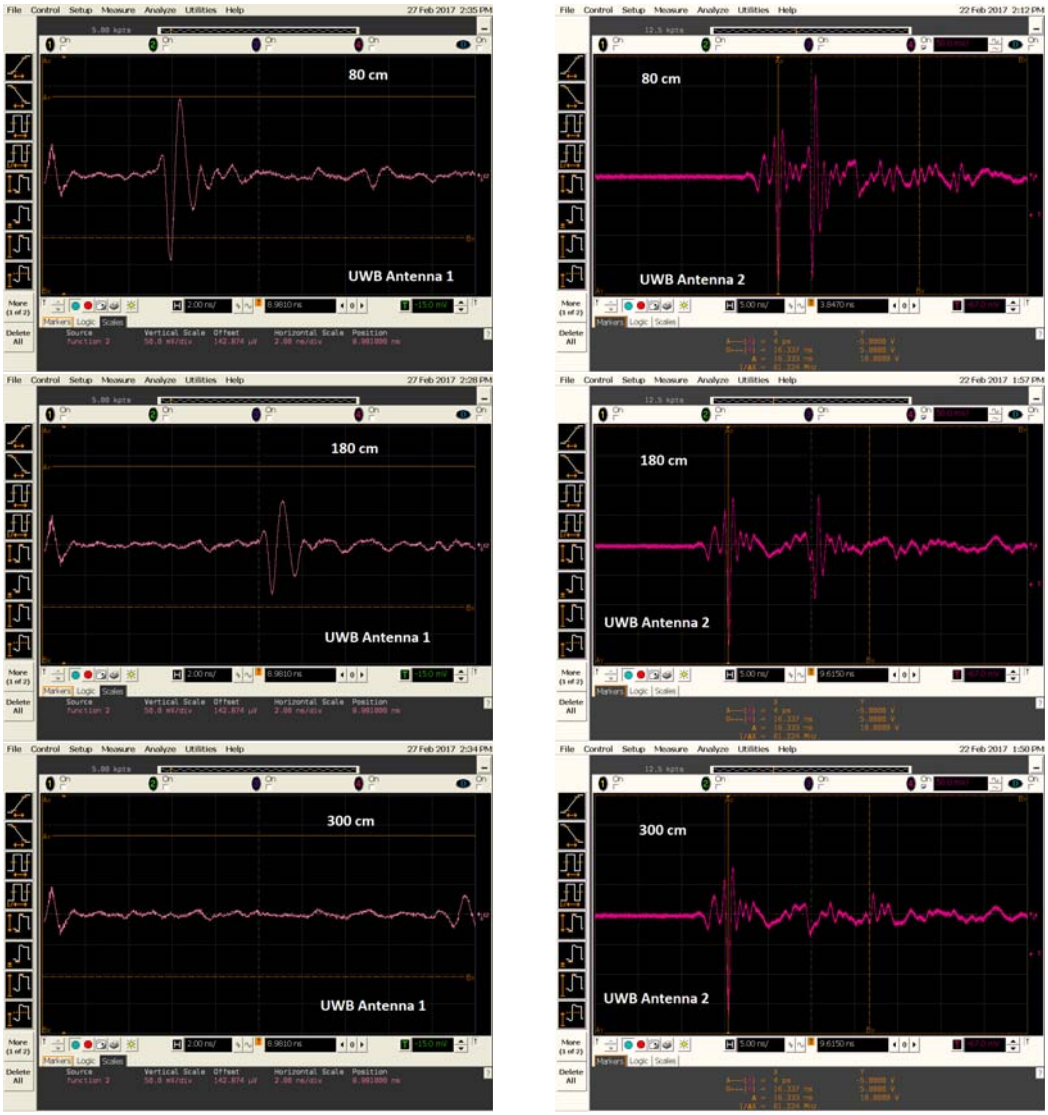

Figure 11. The time-domain response of the radar sensor measurement towards a metal plate located from 80 to 300 cm from two different antennas.

lower frequencies is a very challenging [21–24]. Nevertheless, this work it is focused only on the design of an impulse generator for a radar sensor and demonstrates its workability for measuring the distance and electrical properties for some materials.

3.2. Measurements of Electrical Properties

Secondly, the designed system has been tested for electrical properties measurement towards a lossy dielectric, and the Tapered Slot Antenna has been chosen, because it has a wide bandwidth ranging from 0.46 to 6 GHz and gives better results regarding transmission and reception of pulses. The radar sensor is located in front of a dielectric material, and the antenna was placed orthogonally with a distance of 150 cm from the targets. The relative permittivity of the materials can be measured using a useful procedure; we measure the amplitudes of the signals reflected from a metal plate and from the boundary of the dielectric of the target. We conclude the intrinsic impedance η_1 of the dielectric using Equation (1):

$$\eta_1 = \eta_0 \times \frac{E_m + E_1}{E_m - E_1} \tag{1}$$

where E_m is the amplitudes of the signals reflected from the metal plate, which is equal to the amplitude of the signal incident, E_1 the amplitudes of the signals reflected from the first boundary between air and the top side of the dielectric materials, and $\eta_0 = 377\,\Omega$ the intrinsic impedance of air. Therefore, the relative permittivity ε_{r_1} of the dielectric can be found with Eq. (2):

$$\varepsilon_{r_1} = \frac{377^2}{\eta_1} \tag{2}$$

At first, the measurement of metal with distance of 150 cm was captured in channel 4, and a Low Pass Filter (LPF) with a $fc = 20\,\text{GHz}$ has been applied and saved as function 2 in the Oscilloscope. After that, a measurement from a PVC with LPF has been saved in memory 2; finally, the difference between the function 2 and memory 2 was shown in function 3.

Measurement responses at 150 cm for the metal and the PVC targets are shown in Fig. 12. It is demonstrated that the behaviors of the curves are completely different due to electrical properties of the material.

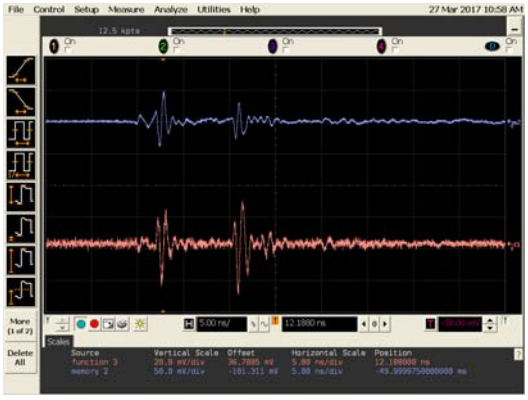

Figure 12. The responses from a metal and PVC at 150 cm.

To validate the functionality of our system, many experiments have been done for different distances in the anechoic chamber in order to avoid electromagnetic perturbations in Fig. 13. Plot the detection measurements for a distance ranging from 80 cm to 300 cm to predict the real part of the dielectric property of the material.

The electrical properties of these materials can be calculated easily using the simple method described above. This method only allows real parts of the complex intrinsic impedance. Nevertheless, although such a simple and approximate measurement procedure was implemented, a good agreement between experimental and theoretical results has been achieved. For this purpose, this simple technique is actually preferred in the most practical issue. Table 1 shows the experimental and theoretical results of the electrical properties.

Table 1.

Materials	Theoretical Results	Experimental Results
Polyvinylchloride (PVC)	4 at 3 GHz	3.7–4.3
Wood	1.5–2 at 3 GHz	1.2–2.2
Teflon (PTFE)	2.0–2.1 at 3 GHz	1.8–2.3

3.3. Range Accuracy

More improvement on the signal reception and better use of data at the response can be taken with a developed signal processing in Matlab, but it is not the principal aim of this paper. Our

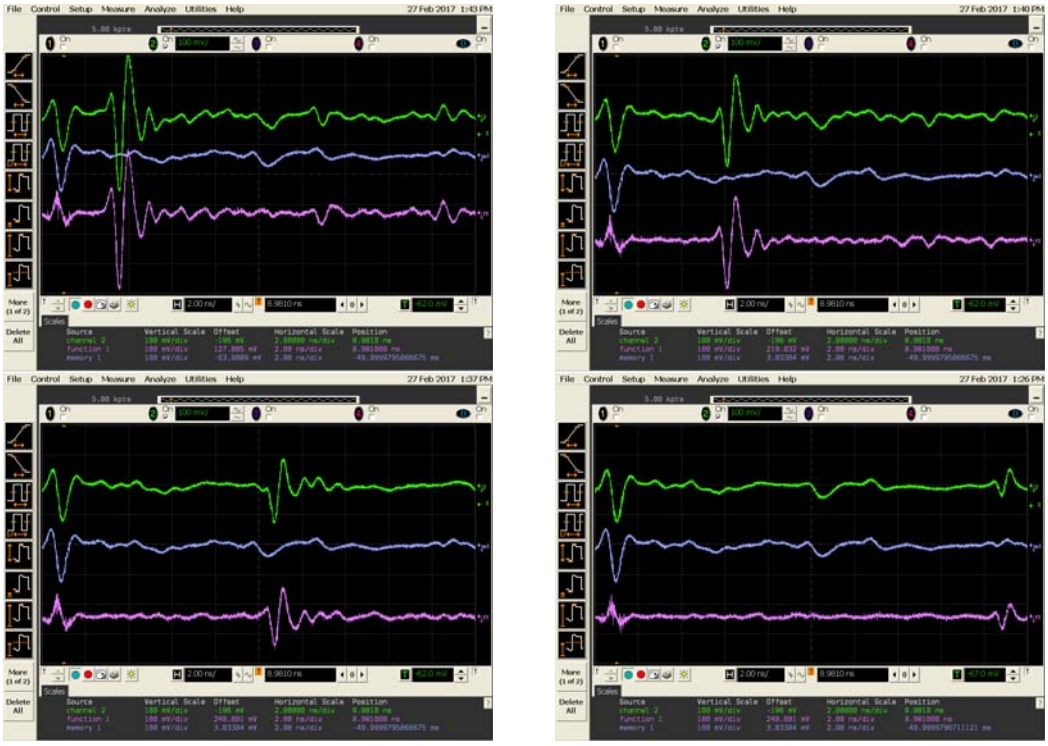

Figure 13. The responses from a metal and PVC in different distances.

purpose was to report the hardware development and to demonstrate the workability of the radar sensor prototype in nondestructive measurements and its precise application in distance and electrical properties measurements. Fig. 14 shows the accuracy variation of measurement according to the change of the location of the target, its proportional quasi-linearity, which makes the our designed impulse generator very attractive specially in court range measurement, and its advantageous in non-contact and nondestructive measurement of distance and the electrical properties of material in such a industrial process.

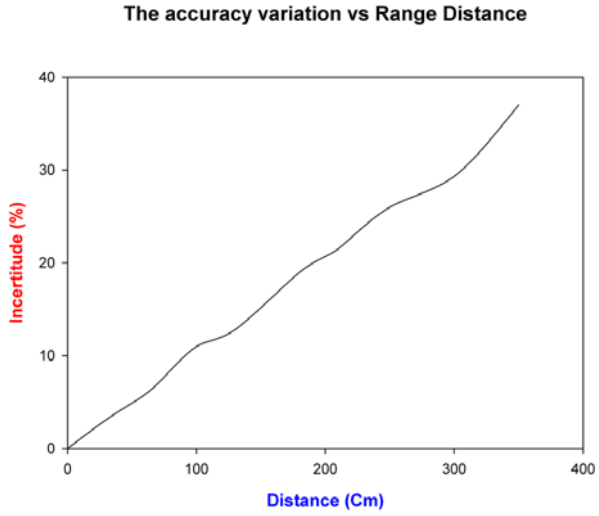

Figure 14. The Variation of accuracy measurements variation with the range distance.

4. CONCLUSION

A useful UWB radar sensor prototype has been developed for NDE applications using all integrated microwave circuits. The UWB radar sensor employs a 333 ps monocycle-pulse transmitter, 0–6 GHz Sampling Receiver (Oscilloscope) and two antennas operating from 460 MHz to at least 6 GHz. A simple mathematical formula has been used to calculate the range distance and the electrical permittivity of materials. Many measurements have been made to confirm the performance and operability of this system prototype. All measurements have been done in an anechoic chamber to avoid interferences with other signals. Experimental data, obtained with the fabricated prototype in measurement procedure demonstrate good agreements with the theoretical results. Good performances, together with compactness and low cost, make this system a desirable and useful tool for NDE applications.

ACKNOWLEDGMENT

The authors gratefully acknowledge the financial support provided by Pierre and Marie Curie University under the EMMAG Scholarship. This study was supported by DIMAS group, ITACA institute at City polytechnic of innovation from university polytechnic of Valencia.

REFERENCES

1. Chabinski, I. J., "Applications of microwave energy. Past, present and future. Brave new worlds," *Proceedings of the Materials Research Society Symposium*, Vol. 124, 17–32, 1990.
2. Baker-Jarvis, J., M. D Janezic, B. F Riddle, C. L. Holloway, N.-G. Painter, and J.-E. Bendell, "Dielectric and conductor loss characterization and measurements on electronic packaging materials," *NIST Technical Note*, Vol. 1520, July 2001.
3. Bruce, R. W., "New frontiers in the use of microwave energy: Power and metrology," *Microwave Processing of Materials, Proceeding of Materials Research Society Symposium*, Vol. 124, 3–15, 1990.
4. Chen, L. F., C. K. Ong, C. P. Neo, V. V. Vardan, and V. K. Vardan, *Microwave Electronics, Measurement and Materials Characterisation*, John Wiley & Sons, Ltd., 2004.
5. Dench, E. C., "Advantages of microwave processing," *Proceeding of the IMPS Symposium*, 1–5, Canada, 1973.
6. Komarov, V., S, Wang, and J. Tang, *Permittivity and Measurement, Encyclopedia of RF and Microwave Engendering*, John Wiley & Sons, Ltd., 2004.
7. Bernardi, P., R. Cicchetti, S. Pisa, E. Pittella, E. Piuzzi, and O. Testa, "Design, realization and test of a UWB radar sensor for breath activity monitoring," *IEEE Sensors Journal*, Vol. 14, No. 2, 584–596, February 2014.
8. Lee, D., J. Velander, D. Nowinski, and R. Augustine, "A preliminary research on skull healing utilizing short pulsed radar technique on layered cranial surgery phantom models," *Progress In Electromagnetics Research C*, Vol. 84, 1–9, 2018.
9. Mohanna, M. M., E. A. Abdallah, H. M. S. El-Hennawy, and M. A. Attia, "Design and analysis of a novel low loss ultra-wideband coplanar waveguide (CPW) to coplanar strips (CPS) transition for tapered slot antennas (TSA) in ground penetrating radar (GPR) application," *Progress In Electromagnetics Research C*, Vol. 83, 179–194, 2018.
10. Xu, X., T. Xia, V. Anbu, and H. Driver, "The development of a high-speed ultra-wide-band ground penetrating radar for rebar detection," *ASCE's Journal of Engineering Mechanics*, Vol. 139, 272–285, 2013.
11. Lu, S., G. Cui, X. Yu, L. Kong, and X. Yang, "Cognitive radar waveform design against signal-dependent modulated jamming," *Progress In Electromagnetics Research B*, Vol. 80, 59–77, 2018.
12. Lee, J. S., C. Nguyen, and T. Scullion, "New uniplanar subnanosecond monocycle pulse generator and transformer for time-domain microwave application," *IEEE Trans. Microwave Theory Tech.*, Vol. 49, 1126–1129, 2001.

13. Ma, T.-G., C.-J. Wu, P. K. Cheng, and C.-F. Chou, "Ultrawideband monocycle pulse generator with dual resistive loaded shunt stubs," *IEEE Microw. Opt. Technol.*, 459–462, 2007.
14. Ruengwaree, A., A. Ghose, J. Weide, and G. Kompa, "Ultra-fast pulse transmitter for UWB microwave radar," *36th European Microwave Conference*, 1833–1836, 2006.
15. Guo, Y., G. Zhu, and Z. Zhou, "A novel design and implementation of sub-nanosecond sampling pulse generator for ultra-wideband equivalent sampling receiver," *Fifth International Conference on Computing, Communications and Networking Technologies (ICCCNT)*, 1–5, 2014.
16. Pongsoon, P., K. Bunnjaweht, and D. Kaemarungsi, "Edge-triggered driver circuit for ultra-wideband pulse generator with cascade impulse shaping," *9th International Conference on Electrical Engineering/Electronics, Computer, Telecommunications and Information Technology (ECTICON)*, 1–4, 2012.
17. Protiva, P., J. Mrkvica, and J. Machac, "High power monocycle pulse generator for through-the-wall radar transmitter," *Proc. IEEE Asia-Pacific Conf. Circuits Syst.*, 2324–2327, 2009.
18. Li, Z., X. X. Lv, Y. F. Long, and T. Qin, "An ultra-wideband monocycle pulse generator with good performance," *Proc. Int. Conf. Computat. Problem-Solving (ICCP)*, 253–254, 2011.
19. Zhu, J., Y. Sun, and H. Fang, "Enhanced characteristic basis function method for solving the monostatic radar cross section of conducting targets," *Progress In Electromagnetics Research M*, Vol. 68, 173–180, 2018.
20. Younes, A., J. M. Catala-Rivera, F. P. Foix, and A. Driouach, "Simple, compact and low-cost pulse transmitter for UWB microwave radar," *Mediterranean Conference on Information & Technologies*, 2015.
21. Amdaouch, I., O. Aghzout, A. Naghar, A. V. Alejos, and F. J. Falcone, "Breast tumor detection system based on a compact UWB antenna design," *Progress In Electromagnetics Research M*, Vol. 64, 123–133, 2018.
22. Borja, B., J. A. Tirado-Mendez, and H. Jardon-Aguilar, "An overview of UWB antennas for microwave imaging systems for cancer detection purposes," *Progress In Electromagnetics Research B*, Vol. 80, 173–198, 2018.
23. Baharuddin, M., V. Wissan, J. T. Sri Sumantyo, and H. Kuze, "Equilateral triangular microstrip antenna for circularly-polarized synthetic aperture radar," *Progress In Electromagnetics Research C*, Vol. 8, 107–120, 2009.
24. Takemura, N. and S. Ichikawa, "Broadbanding of printed bell-shaped monopole antenna by using short stub for UWB applications," *Progress In Electromagnetics Research C*, Vol. 78, 57–67, 2017.